Kusumoto *Earth, Planets and Space* (2016) 68:153
DOI 10.1186/s40623-016-0529-7

Earth, Planets and Space

LETTER Open Access

Dip distribution of Oita–Kumamoto Tectonic Line located in central Kyushu, Japan, estimated by eigenvectors of gravity gradient tensor

Shigekazu Kusumoto*

Abstract: We estimated the dip distribution of Oita–Kumamoto Tectonic Line located in central Kyushu, Japan, by using the dip of the maximum eigenvector of the gravity gradient tensor. A series of earthquakes in Kumamoto and Oita beginning on 14 April 2016 occurred along this tectonic line, the largest of which was $M = 7.3$. Because a gravity gradiometry survey has not been conducted in the study area, we calculated the gravity gradient tensor from the Bouguer gravity anomaly and employed it to the analysis. The general dip distribution of the Oita–Kumamoto Tectonic Line was found to be about 65° and tends to be higher towards its eastern end. In addition, we estimated the dip around the largest earthquake to be about 60° from the gravity gradient tensor. This result agrees with the dip of the earthquake source fault obtained by Global Navigation Satellite System data analysis.

Keywords: Dip distribution, Oita–Kumamoto Tectonic Line, Kumamoto earthquake, Gravity gradient tensor, Eigenvector, Futagawa fault system, Aso caldera, Hohi volcanic zone

Introduction

A series of earthquakes in Kumamoto and Oita began on 14 April 2016 in the areas along the Oita–Kumamoto Tectonic Line in central Kyushu, Japan (Fig. 1). The Oita–Kumamoto Tectonic Line is an area of high horizontal gravity gradient anomaly (e.g. Tsuboi et al. 1956) located at the boundary between Cenozoic volcanic rocks and Palaeozoic and Mesozoic Erathems (e.g. Kamata and Kodama 1993). This tectonic line consists of many active faults (e.g. Research Group for Active Faults 1991).

The central Kyushu area is well known for its active volcanoes and calderas such as the Aso and Shishimuta calderas (e.g. Yokoyama 1963; Kubotera et al. 1969; Komazawa 1995; Kamata 1989). This area also includes the Beppu–Shimabara Graben (Matsumoto 1979) in addition to brisk seismic activities with focal mechanisms of lateral faulting, normal faulting or both (e.g. Shimizu et al. 1993; Sudo 1993). The strain field in Kyushu during the last 100 years, which was obtained by geodetic survey, indicates N–S extension (Tada 1984). Matsumoto et al. (2015) reported that the stress condition determined by focal mechanisms in the seismogenic layer, shallower than 30 km, has compressive and tensile axes of WSW–ENE and NNW–SSE directions. They also reported that the seismicity around the shear zone at the southern edge of the Beppu–Shimabara Graben is strike-slip faulting and that in the graben is normal faulting.

In general, subsurface structures play important roles in the understanding and discussion of tectonics of active areas. Frequently employed geophysical survey methods in these volcanic areas include geoelectromagnetic and gravity surveys (e.g. Mogi and Nakama 1993; Komazawa 1995; Kusumoto et al. 1996; Handa 2005). In recent years, gravity gradiometry has been introduced (e.g. Jekeli 1988; Dransfield 2010; Chowdhury and Cevallos 2013; Braga et al. 2014).

This type of survey observes a gravity gradient tensor consisting of six components of three-dimensional (3-D) gradients of gravitation by a causative body and has higher sensitivity than gravity surveys. Various analysis

*Correspondence: kusu@sci.u-toyama.ac.jp
Graduate School of Science and Engineering for Research (Science), University of Toyama, 3910 Gofuku, Toyama 930-8555, Japan

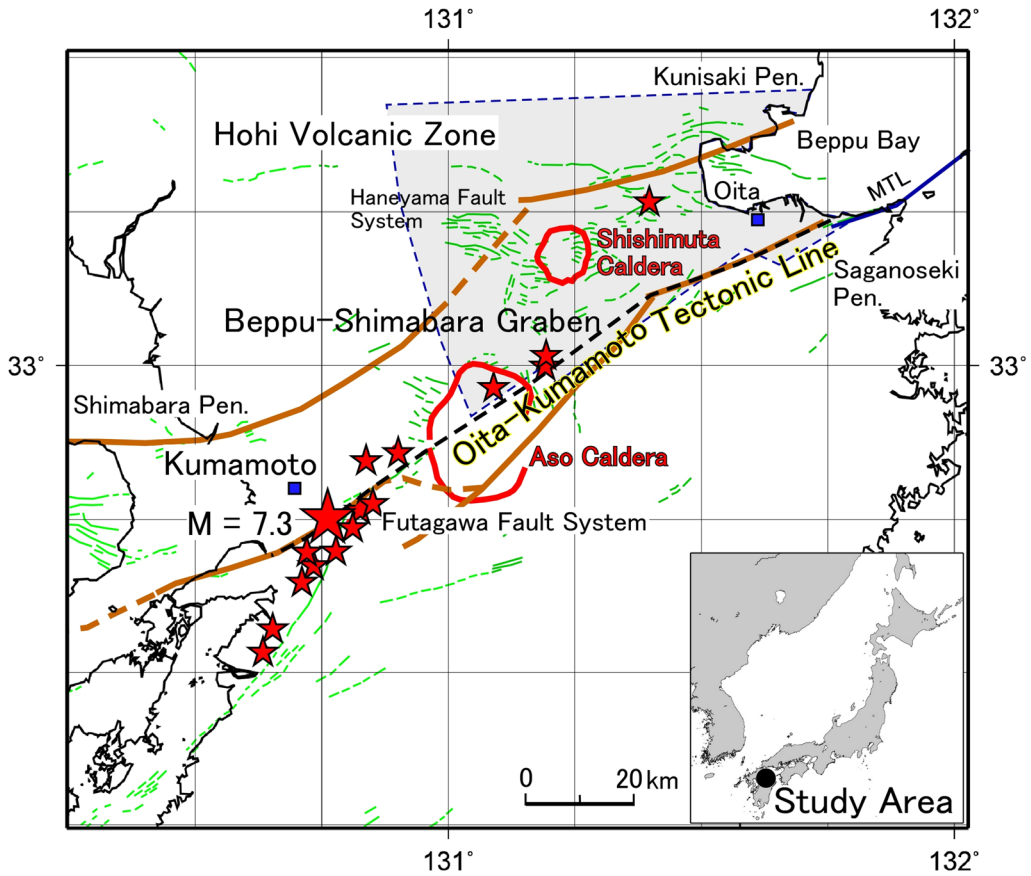

Fig. 1 Location map of study area. The *black dashed line* is the Oita–Kumamoto Tectonic Line, and the *blue line* is the Median Tectonic Line (MTL), which is the largest tectonic line with a right-lateral fault component in south-western Japan. The *light grey* area with *blue dashed line* indicates the Hohi volcanic zone (Kamata 1989). The area between ochreous lines is the Beppu–Shimabara Graben (Matsumoto 1979). *Red lines* indicate the calderas; *green lines* are active faults (e.g. Research Group for Active Faults 1991), and *red stars* indicate epicentres of which the magnitude was more than 5 in earthquakes occurring between 14 April and 19 April 2016

techniques using gravity gradient tensors have been developed and have given excellent results in subsurface structure estimations and edge detections (e.g. Zhang et al. 2000; Beiki 2010; Martinez et al. 2013; Cevallos 2014; Li 2015). In the recent years, techniques estimating the dip of a geological structure boundary by using the gradient tensor of the potential fields have been developed and have shown good results (e.g. Beiki 2013; Kusumoto 2015, 2016; Itoh et al. 2016). The dip of the structure plays an important role in numerical simulations that quantitatively examine tectonics (e.g. Finch et al. 2004; Itoh et al. 2014; Kusumoto et al. 2015).

In this paper, as a quick report, we show the dip distribution of the Oita–Kumamoto Tectonic Line estimated by the technique suggested by Beiki (2013) and Kusumoto (2015). With the exception of some geothermal areas, gravity gradiometry survey has not been conducted thus far in central Kyushu. Therefore, we estimated the gravity gradient tensor by using calculations based on Mickus and Hinojosa (2001) to obtain the tensor from the gravity anomaly, which was used for this study.

Gravity anomaly and gravity gradient tensor

Figure 2 shows the residual Bouguer gravity anomaly map of which the first trend surface was removed from the original Bouguer gravity anomaly by using the least squares method in order to eliminate the effect of the subducting plate. A Bouguer density of 2670 kg/m^3 was employed here. In this study, the gravity anomaly database by Komazawa (2004) was employed. Because this database provides mesh data with intervals of 1 km × 1 km, we discuss structures larger than several kilometres.

The figure indicates negative gravity anomalies caused by the Shishimuta and Aso calderas and some tectonic sedimentary basins such as Beppu Bay. In addition, high horizontal gravity gradient belts caused by the Median Tectonic Line and the Oita–Kumamoto Tectonic Line are

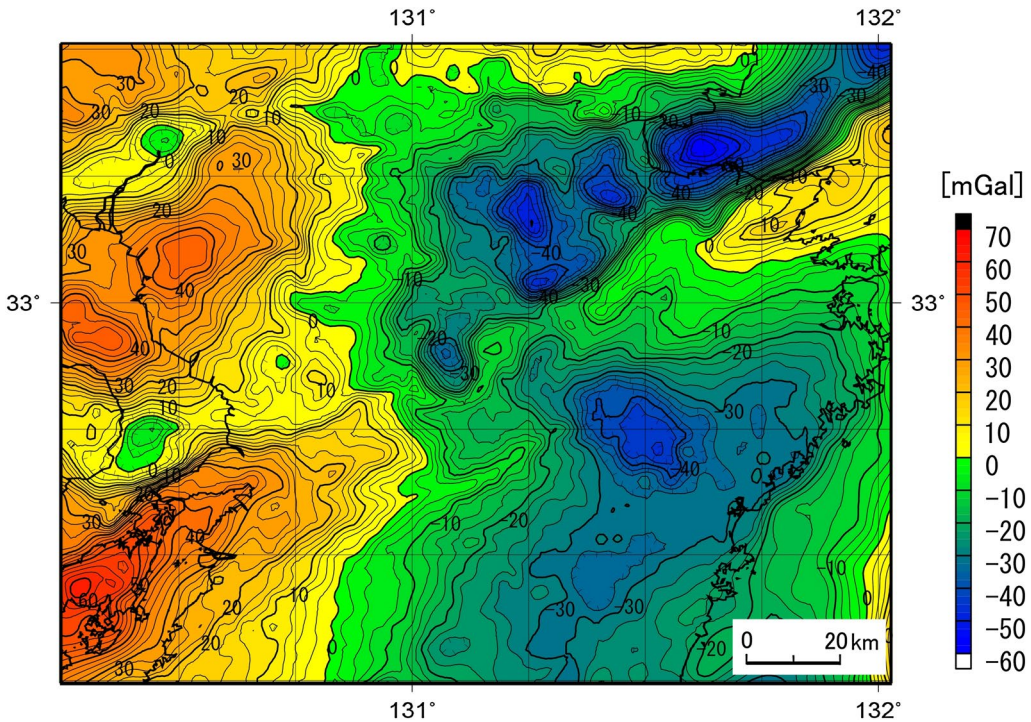

Fig. 2 Residual Bouguer gravity anomaly map of the study area. The contour interval is 2.5 mGal. In this map, the regional linear trend of the Bouguer gravity anomalies such as the effect of the subducting plate was estimated and removed by using the least squares method. The Bouguer gravity anomaly used here is based on the gravity anomaly database (1 km × 1 km mesh data) of Komazawa (2004); a Bouguer density of 2670 kg/m^3 was employed

shown. The Beppu–Shimabara Graben shown in Fig. 1 corresponds to the negative gravity anomaly area in the north-east and to a gravity low area less than about 20 mGal in the south-west.

The gravity gradient tensor Γ is defined on the basis of differential coefficients of the gravity potential (e.g. Torge 1989; Hofmann-Wellenhof and Moritz 2005). Defining g_x, g_y, g_z as the first derivative of the gravity potential along the x-, y-, and z-directions, the gravity gradient tensor Γ is shown as

$$\Gamma = \begin{bmatrix} \frac{\partial g_x}{\partial x} & \frac{\partial g_x}{\partial y} & \frac{\partial g_x}{\partial z} \\ \frac{\partial g_y}{\partial x} & \frac{\partial g_y}{\partial y} & \frac{\partial g_y}{\partial z} \\ \frac{\partial g_z}{\partial x} & \frac{\partial g_z}{\partial y} & \frac{\partial g_z}{\partial z} \end{bmatrix} = \begin{bmatrix} g_{xx} & g_{xy} & g_{xz} \\ g_{yx} & g_{yy} & g_{yz} \\ g_{zx} & g_{zy} & g_{zz} \end{bmatrix}. \quad (1)$$

Here, g_z is the gravity anomaly, and g_{zz} is the vertical gradient of the gravity anomaly. The gravity gradient tensor is symmetric (e.g. Torge 1989), and the sum of its diagonal components is zero because the gravity potential satisfies the Laplace equation.

Although the gravity gradient tensor is generally measured by gravity gradiometry (e.g. Lee 2001; Barnes and Lumley 2011; Dransfield and Christensen 2013), the tensor can be obtained from the gravity anomaly data by using calculations shown in Mickus and Hinojosa (2001). Mickus and Hinojosa (2001) showed the following procedures: (1) apply a 2-D Fourier transformation to the gravity anomaly; (2) estimate the gravity potential by integration of the gravity anomaly in the Fourier domain; (3) calculate the gravity gradient components by second-order derivatives of the potential in each direction; and (4) apply a 2-D Fourier inverse transformation to finally obtain all components of the tensor in the spatial domain. Integration and differentiation of a function in the Fourier domain are equivalent to division and multiplication by powers of wave number (e.g. Blakely 1996).

This method is excellent and mathematically sound. However, because the second-order derivatives of the potential in the Fourier domain and Fourier inverse transformation emphasise short wavelength signals including noise, we obtained components of the gravity gradient tensor by numerical differentiation of g_x, g_y, and g_z in the space domain. The components of g_x and g_y were calculated by the method of Mickus and Hinojosa (2001). The horizontal derivatives of g_x, g_y, and g_z were calculated using simple finite-difference methods (e.g. Blakely 1996). The vertical gravity gradient, g_{zz}, has been computed as

$g_{zz} = -(g_{xx} + g_{yy})$, since the gravity potential satisfies the Laplace's equation.

In the analysis of subsurface structures using the gravity gradient tensor, the horizontal gravity gradient method is the most widely used for finding structure boundaries such as faults or contacts between different materials (e.g. Blakely and Simpson 1986; Shichi et al. 1992; Kudo and Kono 1999; Yamamoto 2003). The horizontal gravity gradient (HG) is given using the components of the tensor shown in Eq. (1) as

$$\mathrm{HG} = \sqrt{g_{zx}^2 + g_{zy}^2}. \tag{2}$$

Figure 3a shows a map of the horizontal gravity gradient. Figure 3b shows areas of more than 25 E (Eötvös: 1 E = 0.1 mGal/km) from which structural boundaries such as the outlines of the Median Tectonic Line, Oita–Kumamoto Tectonic Line, Shishimuta and Aso calderas are extracted. It was found that a series of earthquakes occurred on the high gravity gradient belt. At the western terminations of the Median Tectonic Line and of the Futagawa fault system belonging to the Oita–Kumamoto Tectonic Line, steep gravity gradient areas reach 100 E.

Dip estimation of fault or density structure boundary

Because the maximum eigenvector (v_1) of the gradient tensor of the potential field indicates the direction of the causative body (Beiki and Pedersen 2010), Beiki (2013) suggested that the dip of the causative body can be estimated from the respective x, y, and z components (v_{1x}, v_{1y}, v_{1z}) of the maximum eigenvector, v_1, as follows:

$$\alpha = \arctan\left[\frac{v_{1z}}{\sqrt{(v_{1x})^2 + (v_{1y})^2}}\right], \tag{3}$$

This equation is valid in estimating the dip of the causative body if the body is a 2-D structure like a dyke as shown in Fig. 4a. Structural characteristics of subsurface structure can be evaluated by a dimensionality index. Since the index is <0.5 if the body causing a gravity anomaly is a 2-D structure, it is recommended that this calculation would be conducted under the condition of a dimensionality index of <0.5 (Beiki and Pedersen 2010; Beiki 2013). The dimensionality index (DI) is defined as (Perdersen and Rasmussen 1990)

$$\mathrm{DI} = \frac{-27I_2^2}{4I_1^3}. \tag{4}$$

Here, I_1 and I_2 are invariants of the gravity gradient tensor. Each invariant is given by three eigenvalues (λ_1, λ_2, λ_3) of the tensor as follows:

$$\begin{aligned} I_1 &= \lambda_1\lambda_2 + \lambda_2\lambda_3 + \lambda_1\lambda_3 \\ I_2 &= \lambda_1\lambda_2\lambda_3 \end{aligned}. \tag{5}$$

Kusumoto (2015) considered that a basement consists of an assembly of high-density columns (Fig. 4b) and applied this idea to analysis of fault dip. To effectively estimate the dip of the fault or density structure boundary, Kusumoto (2015) recommended that the estimation would be conducted at areas of high horizontal gravity gradient. In this study, the dip of the structure boundary was estimated in the area satisfying the conditions of which tectonic lines are extracted precisely and are 2-D structure, namely the areas of HG $\geq$ 25 E and DI $\leq$ 0.5.

Results and discussion

Figure 5 shows the estimated dip distribution of large structure boundaries recognised by high horizontal gravity gradient anomalies. The dips of the Median Tectonic Line and Oita–Kumamoto Tectonic Line ranged from of 30° to 80° and were estimated as high-angle tectonic lines or an assembly of high-angle faults. In addition, the dip of the caldera wall of the Aso caldera was estimated to be 50°–70°.

In part of the Median Tectonic Line, the dip is very high and exceeds 70° in some areas. It is well known that the Median Tectonic Line had moved as a right-lateral fault in the Quaternary; thus, the high dips reaching 70° or 80° are expected. The dips of the Median Tectonic Line become low gradually to the north in the Beppu Bay area. Although Kusumoto (2015) reported that this dip estimation technique tends to underestimate the actual dip in deep parts when applied to normal faults, seismic reflection surveys have confirmed dips of normal faults distributed in Beppu Bay to be 17° and 7° by seismic reflection surveys (e.g. Itoh et al. 2014). Therefore, the dip distribution calculated from the gravity gradient tensor agrees with the observed data.

In part of the Oita–Kumamoto Tectonic Line, the general dip was estimated to be about 65°. Because large-scale seismic survey has not been conducted around this tectonic line, its actual dip is unknown. However, the dip estimated from the gravity gradient tensor agrees with the fault dip obtained from crustal movement due to an earthquake in the Futagawa fault system.

The largest earthquake, $M = 7.3$, occurred on 15 April 2016 in a series of earthquakes at the centre of the Futagawa fault system; its fault parameters are estimated from crustal movement data observed by GNSS (The Headquarters for Earthquake Research Promotion 2016). According to The Headquarters for Earthquake Research Promotion (2016), the earthquake source fault is right lateral with a normal fault component, and the upper depth, length, width, azimuth, dip, slip angle, and slip

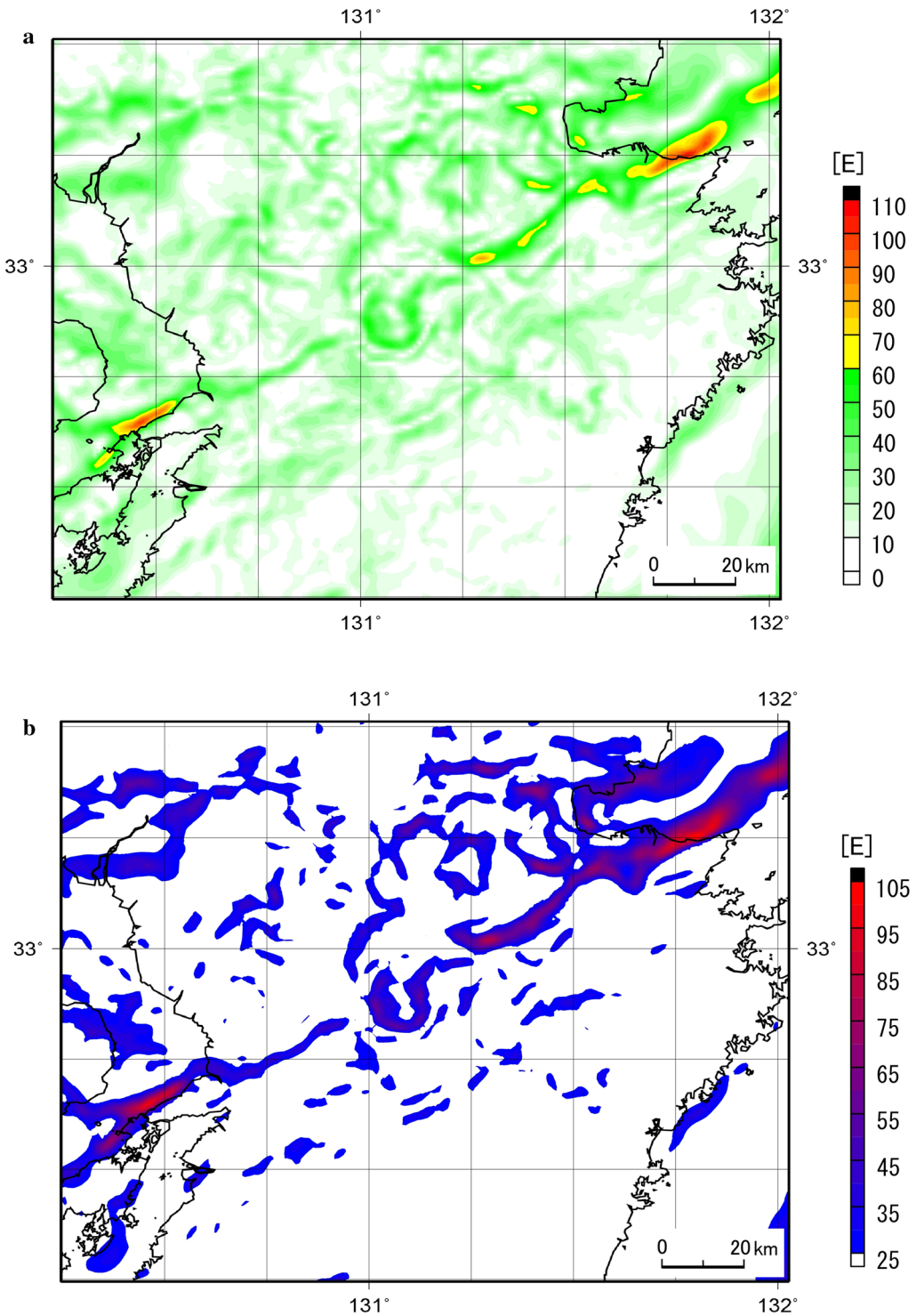

Fig. 3 Horizontal gravity gradient map. **a** Horizontal gravity gradient map of which all data are shown; the contour interval is 10 E (Eötvös: 1 E = 0.1 mGal/km). **b** Horizontal gravity gradient map of which areas of more than 25 E are shown by coloured contours; the contour interval is 5 E

amount of the fault are estimated to be 0.1, 27.1, 12.3 km, 235°, 60°, −161°, and 3.5 m, respectively. Figure 5 shows that the dips estimated from the gravity gradient tensor are 30°–40° at the northern side and roughly 55°–65° at the southern side. Because the earthquake source fault dips to the north, and this technique tends underestimate

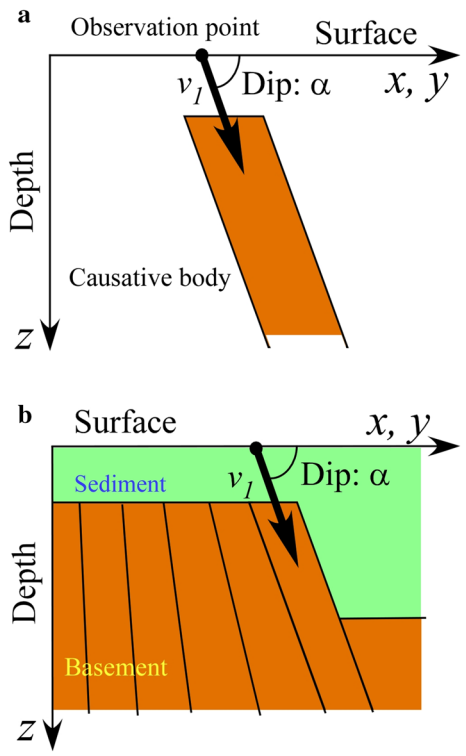

Fig. 4 Schematic illustration of the eigenvectors for two-dimensional (2-D) structures such as dykes and faults. **a** Basic model. In this figure, v_1 is the maximum eigenvectors of the gravity gradient tensor and points to the causative body. The angle *a* between the surface and the maximum eigenvector is the dip of the causative body. **b** Fault dip model. A basement consists of an assembly of high-density columns, and the angle, *a*, indicates the fault dip

the actual dip in deep part for normal faults, the dips estimated from the gravity gradient tensor were found to agree with the fault dip obtained by crustal movement in the central eastern part of the Futagawa fault system.

From these discussions, it appears that the dip estimation technique using eigenvectors and eigenvalues of the gravity gradient tensor effectively provided the dip of the Oita–Kumamoto Tectonic Line, which we conclude to be generally about 65°. In detail, the dip of the Oita–Kumamoto Tectonic Line tends to be higher towards its eastern end and exceeds 70° at the area connecting to the Median Tectonic Line. The dip in the Futagawa fault system area is relatively low at about 60°. This variation or trend is divided into eastern and western areas by the Aso caldera. Although a series of earthquakes occurred along the Oita–Kumamoto Tectonic Line, the cause or origin and formation processes of this tectonic line might be different in each segment.

Although the tectonics in the western part of the Aso caldera are unknown in detail, the eastern part of the Aso caldera is known as the Hohi volcanic zone (e.g. Kamata 1989), which consists of a half-graben with volcanic activities that began in 6 Ma (e.g. Kamata 1989) and pull-apart basins that were formed after the half-graben formation in about 1.5 Ma (e.g. Itoh et al. 1998). These structures and their formation processes have been restored by numerical simulations assuming high-dip (80°) normal faulting and right-lateral faulting (e.g. Kusumoto et al. 1999). It appears that the formation of the half-graben in 6 Ma plays an important role in understanding the spatial variation of dip distribution because the Oita–Kumamoto Tectonic Line is the boundary between Cenozoic volcanic rocks and Palaeozoic and Mesozoic Erathems.

In this study, we used the existing gravity anomaly database (Komazawa 2004) which compiled 1 km × 1 km mesh data of the Bouguer gravity anomaly obtained by Bouguer density of 2670 kg/m^3. Although changes of the mesh size and the Bouguer density vary aspects of some maps, it seems that they would not make serious differences in the general situation. However, to obtain a detailed fault shape and to discuss the cause of a series of earthquakes tectonically, in addition to discussions on change of the Bouguer density, it is effective to use a dense gravity database or to conduct gravity gradiometer survey and seismic reflection survey around fault zones in the future studies.

Conclusion

In this study, we estimated the dip distribution of the Oita–Kumamoto Tectonic Line where a series of earthquakes began on 14 April 2016. For dip estimation, the method using the dip of the maximum eigenvector of the gravity gradient tensor was employed. Because gravity gradiometry survey has not been conducted in the study area, the tensor was obtained by calculations from the Bouguer gravity anomaly. The estimation was conducted in an area satisfying the following conditions: (1) a horizontal gravity gradient larger than 25 E and (2) a dimensionality index <0.5.

We obtained that the dip of the Oita–Kumamoto Tectonic Line is generally about 65°. The fault dip around the largest earthquake of $M = 7.3$ in a series of earthquakes was estimated to be about 60°, which agrees with the dip of the earthquake source fault obtained by GNSS data analysis.

In addition, we found that the dip distribution of the Oita–Kumamoto Tectonic Line tends to be higher towards its eastern end, exceeding 70° at the area connecting with the Median Tectonic Line. On the other hand, the dip in the Futagawa fault system area is relatively low. This spatial variation of dip distribution has been attributed to the formation of a half-graben with volcanic activities that began in 6 Ma. However, more observations and discussions including numerical

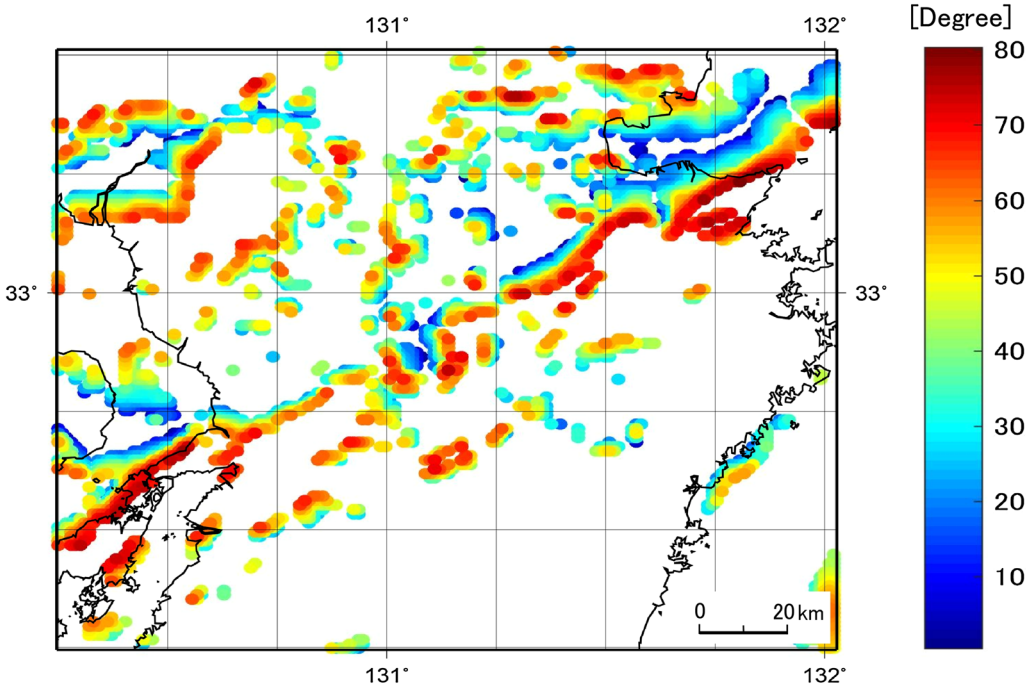

Fig. 5 Distribution of estimated dip of faults or structural boundaries. Dip estimations were conducted for the areas satisfying the conditions (DI) <0.5 and horizontal gravity gradient (HG) ≥25 E

simulations are needed to understand these results because details of the tectonics in the Futagawa fault system area are unknown.

Acknowledgements
This work was supported partially by the Integrated Research for Beppu—Haneyama Fault Zone (East part of Oita Plain—Yufuin Fault) by MEXT and by JSPS (Japan Society for the Promotion of Science) KAKENHI Grant Number 15K14274. The author is grateful to these agencies. Lastly, we are most grateful to two anonymous reviewers for their constructive reviews and comments on the manuscript and to Hiroyuki Tsutsumi for his editorial advice and cooperation.

Competing interests
The author declares that he has no competing interests.

Received: 17 June 2016 Accepted: 27 August 2016
Published online: 06 September 2016

References

Barnes G, Lumley J (2011) Processing gravity gradient data. Geophysics 76:I33–I47
Beiki M (2010) Analytic signals of gravity gradient tensor and their application to estimate source location. Geophysics 75:I59–I74
Beiki M (2013) TSVD analysis of Euler deconvolution to improve estimating magnetic source parameters: an example from the Asele area, Sweden. J Appl Geophys 90:82–91
Beiki M, Pedersen LB (2010) Eigenvector analysis of gravity gradient tensor to locate geologic bodies. Geophysics 75:I37–I49
Blakely RJ (1996) Potential theory in gravity and magnetic applications. Cambridge University Press, Cambridge
Blakely R, Simpson RW (1986) Approximating edges of source bodies from magnetic or gravity anomalies. Geophysics 51:1494–1498
Braga MA, Endo I, Galbiatti HF, Carlos DU (2014) 3D full tensor gradiometry and Falcon systems data analysis for iron ore exploration: Bau Mine, Quadrilatero Ferrifero, Minas Gerais, Brazil. Geophysics 79:B213–B220
Cevallos C (2014) Automatic generation of 3D geophysical models using curvatures derived from airborne gravity gradient data. Geophysics 79:G49–G58
Chowdhury PR, Cevallos C (2013) Geometric shapes derived from airborne gravity gradiometry data: new tools for the explorationist. Lead Edge 32:1468–1474
Dransfield M (2010) Conforming Falcon gravity and the global gravity anomaly. Geophys Prospect 58:469–483
Dransfield MH, Christensen AN (2013) Performance of airborne gravity gradiometers. Lead Edge 32:908–922
Finch E, Hardy S, Gawthorpe R (2004) Discrete-element modelling of extensional fault propagation folding above rigid basement fault blocks. Basin Res 16:489–506. doi:10.1111/j.1365-2117.2004.00241.x
Handa S (2005) Electrical conductivity structures estimated by thin sheet inversion, with special attention to the Beppu–Shimabara graben in central Kyushu, Japan. Earth Planets Space 57:605–612
Hofmann-wellenhof B, Moritz H (2005) Physical geodesy. Springer, Berlin
Itoh Y, Takemura K, Kamata H (1998) History of basin formation and tectonic evolution at the termination of a large transcurrent fault system: deformation mode of central Kyushu, Japan. Tectonophysics 284:135–150
Itoh Y, Kusumoto S, Takemura K (2014) Evolutionary process of the Beppu Bay in central Kyushu, Japan: a quantitative study of basin-forming process under the control of plate convergence modes. Earth Planets Space 66:74. doi:10.1186/1880-5981-66-74
Itoh Y, Kusumoto S, Takemura K (2016) Research frontiers of sedimentary basin interiors: methodological review and a case study on an oblique convergent margin. Nova Science Pub. Inc., New York
Jekeli C (1988) The gravity gradiometer survey system (GGSS). EOS Trans AGU 69:105
Kamata H (1989) Volcanic and structural history of the Hohi volcanic zone, central Kyushu, Japan. Bull Volcanol 51:315–332

Kamata H, Kodama K (1993) The Hohi volcanic zone as a volcano-tectonic depression and its formation tectonics: three tectonic events caused by subduction of the Philippine Sea plate under the junction of the Southwest Japan Arc and the Ryukyu Arc. Mem Geol Soc Jpn 41:129–148 **(in Japanese with English abstract)**

Komazawa M (1995) Gravimetric analysis of Aso volcanoes and its interpretation. J Geod Soc Jpn 41:17–45

Komazawa M (2004) Gravity grid database of Japan. ver. 2, Digital Geoscience Map P-2 [CD-ROM]. Tsukuba: Geological Survey of Japan

Kubotera A, Tajima H, Sumitomo N, Doi H, Izutuya S (1969) Gravity surveys on Aso and Kuju volcanic region, Kyushu District, Japan. Bull Earthq Res Inst Univ Tokyo 47:215–225

Kudo T, Kono Y (1999) Relationship between distributions of shallow earthquakes and gradient of gravity anomaly field in southwest Japan. Zisin Ser 2(52):341–350 **(in Japanese with English abstract)**

Kusumoto S (2015) Estimation of dip angle of fault or structural boundary by eigenvectors of gravity gradient tensors. Butsuri Tansa 68:277–287 **(in Japanese with English abstract)**

Kusumoto S (2016) Structural analysis of caldera and buried caldera by semi-automatic interpretation techniques using gravity gradient tensor: a case study in central Kyushu Japan. In: Nemeth K (ed) Updates in Volcanology-From volcano modelling to volcano geology. InTech, Rijeka

Kusumoto S, Fukuda Y, Takemoto S, Yusa Y (1996) Three-dimensional subsurface structure in the eastern part of the Beppu–Shimabara Graben, Kyushu, Japan, as revealed by gravimetric data. J Geod Soc Jpn 42:167–181

Kusumoto S, Takemura K, Fukuda Y, Takemoto S (1999) Restoration of the depression structure at the eastern part of central Kyushu, Japan by means of dislocation modeling. Tectonophysics 302:287–296

Kusumoto S, Itoh Y, Takemura K, Iwata T (2015) Displacement fields of sedimentary layers controlled by fault parameters: the discrete element method of controlling basement motions by dislocation solutions. Earth Sci 4:89–94

Lee JB (2001) Falcon gravity gradiometer technology. Explor Geophys 32:247–250

Li X (2015) Curvature of a geometric surface and curvature of gravity and magnetic anomalies. Geophysics 80:G15–G26

Martinez C, Li Y, Krahenbuhl R, Braga MA (2013) 3D inversion of airborne gravity gradiometry data in mineral exploration: a case study in the Quadrilatero Ferrifero, Brazil. Geophysics 78:B1–B11

Matsumoto Y (1979) Some problems on volcanic activities and depression structures in Kyushu, Japan. Mem Geol Soc Jpn 16:127–139 **(in Japanese with English abstract)**

Matsumoto S, Nakao S, Ohkura T, Miyazaki M, Shimizu H, Abe Y, Inoue H, Nakamoto M, Yoshikawa S, Yamashita Y (2015) Spatial heterogeneities in tectonic stress in Kyushu, Japan and their relation to a major shear zone. Earth Planets Space 67:172

Mickus KL, Hinojosa JH (2001) The complete gravity gradient tensor derived from the vertical component of gravity: a Fourier transform technique. J Appl Geophys 46:159–174

Mogi T, Nakama K (1993) Magnetotelluric interpretation of the geothermal system of the Kuju volcano, southwest Japan. J Volcanol Geotherm Res 56:297–308

Perdersen LB, Rasmussen TM (1990) The gradient tensor of potential field anomalies: some implications on data collection and data processing of maps. Geophysics 55:1558–1566

Research Group for Active Faults (1991) The active faults in Japan: sheet maps and inventories, Revth edn. Univ. Tokyo press, Tokyo

Shichi R, Yamamoto A, Kimura A, Aoki H (1992) Gravimetric evidences for active faults around Mt. Ontake, central Japan: specifically for the hidden faulting of the 1984 Western Nagano Prefecture Earthquake. J Phys Earth 40:459–478

Shimizu H, Umakoshi K, Matsuwo N (1993) Seismic activity in middle and western Kyushu. Mem Geol Soc Jpn 41:13–18 **(in Japanese with English abstract)**

Sudo Y (1993) Seismic activity and tectonic significance near the volcanic areas in central Kyushu, Japan. Mem Geol Soc Jpn 41:19–34 **(in Japanese with English abstract)**

Tada T (1984) Spreading of the Okinawa trough and its relation to the crustal deformation in Kyusyu. Zisin Ser 2(37):407–415 **(in Japanese with English abstract)**

The Headquarters for Earthquake Research Promotion (2016) Information on the Kumamoto earthquake. In: The headquarters for earthquake research promotion web site. http://www.static.jishin.go.jp/resource/monthly/2016/2016_kumamoto_2.pdf. Accessed 8 May 2016

Torge W (1989) Gravimetry. Walter de Gruyter, Berlin

Tsuboi C, Jitsukawa A, Tajima H (1956) Gravity survey along the lines of precise levels throughout Japan by means of a Worden gravimeter. Bull Earthq Res Inst Univ Tokyo IV(8):476–552

Yamamoto A (2003) Gravity anomaly atlas of the Ishikari Plain and its vicinity, Hokkaido, Japan. Geophys Bull Hokkaido 66:33–62 **(in Japanese with English abstract)**

Yokoyama I (1963) Structure of caldera and gravity anomaly. Bull Volcanol 26:67–73

Zhang C, Mushayandebvu MF, Reid AB, Fairhead JD, Odegrad ME (2000) Euler deconvolution of gravity tensor gradient data. Geophysics 65:512–520